Paper

Int'l J. of Aeronautical & Space Sci. 18(3), 535–544 (2017)
DOI: http://dx.doi.org/10.5139/IJASS.2017.18.3.535

IJASS
International Journal of Aeronautical and Space Sciences

An Improved Hybrid Kalman Filter Design for Aircraft Engine based on a Velocity-Based LPV Framework

Xiaofeng Liu*

School of Transportation Science and Engineering, Beihang University, Beijing 100191, China

Abstract

In-flight aircraft engine performance estimation is one of the key techniques for advanced intelligent engine control and in-flight fault detection, isolation and accommodation. This paper detailed the current performance degradation estimation methods, and an improved hybrid Kalman filter via velocity-based LPV (VLPV) framework for these needs is proposed in this paper. Composed of a nonlinear on-board model (NOBM) and VLPV, the filter shows a hybrid architecture. The outputs of NOBM are used for the baseline of the VLPV Kalman filter, while the system performance degradation factors on-line estimated by the measured real system output deviations are fed back to the NOBM for its updating. In addition, the setting of the process and measurement noise covariance matrices' values are also discussed. By applying it to a commercial turbofan engine, simulation results show the efficiency.

Key words: Aircraft engine, Hybrid Kalman filter, Linear parameter-varying, Performance estimation

1. Introduction

Aircraft engines can be operated with enhanced efficiency while ensuring safe operation if performance parameters, such as thrust and compressor stall margin, are known. Since these performance parameters are not directly measurable during flight, they can only be controlled indirectly through the utilization of measurable variables in the feedback control architecture. However, under extreme conditions and/or events, aircraft engines safety margins may be compromised.

Accurate in-flight estimation of aircraft engines performance parameters is, therefore, desired to advance the feedback control strategy and consequently enhance aircraft engine safety and efficiency. Some researchers have investigated the application of on-board engine models for the estimation of performance parameters [1, 2]. An on-board model can be a linear or nonlinear representation of the physical aircraft engine, and it can compute non-measurable parameters.

Since an on-board model represents the "nominal" engine, it must be adapted to the performance of the real engine as it deviates from the nominal baseline with time. A well-known approach for adapting an on-board model to an off-nominal engine is to estimate health parameters, such as efficiency, flow capacity, by using the Kalman filter [3, 4]. They deviate from the nominal baseline gradually with time due to normal usage and also abruptly due to component fault events.

The Kalman filter is an efficient recursive filter that estimates the internal state of a linear dynamic system from a series of noisy measurements. The algorithm works in a two-step process. In the prediction step, the Kalman filter produces estimates of the current state variables, along with their uncertainties. Once the outcome of the next measurement (necessarily corrupted with some amount of error, including random noise) is observed, these estimates are updated using a weighted average, with more weight being given to estimates with higher certainty. Because of the algorithm's recursive nature, it can run in real time using only the present input measurements and the previously calculated state and its uncertainty matrix; no additional past information is required. A challenging aspect of this estimation approach is that the linearization approximation problem of nonlinear

* Associate professor, Corresponding author: liuxf@buaa.edu.cn

Received: July 13, 2016 Revised: August 2, 2017 Accepted: August 11, 2017

http://ijass.org pISSN: 2093-274x eISSN: 2093-2480

system within Kalman filter equations' application. That is to solve the nonlinear filter problem, the system's linearization model has to be updated in real time, and it increases the amount of calculation and complexity of the Kalman filter algorithm.

If a Kalman filter is able to accurately estimate all of the health parameters in real time, the Kalman filter can adapt itself to operate in the vicinity of the degraded engine. This approach, however, requires the following condition: the number of sensors must be at least equal to the number of health parameters[5]. In general, this requirement is not met for aircraft engines. Moreover, even if this requirement is met and thus all health parameters are estimated, there are various factors that can cause some problems in estimating health parameters with high accuracy. Examples of such factors are improper sensor location for health parameter estimation, existence of biases in sensors and actuators, and inherent model-plant mismatch. Therefore, the adaptation of the Kalman filter to the degraded engine through the real-time estimation of health parameters is a challenging problem.

Because of the necessity to account for health degradation of a real engine, and for the difficulty in achieving inflight, real-time adaptation of the Kalman filter through health parameter estimation, an alternative approach must be considered. One approach is to periodically update the Kalman filter based on the health condition estimated by some other means. Through the health baseline updates, the performance of the Kalman filter can be maintained in the presence of health degradation.

Actually, almost all real systems present the nonlinear behaviors, and there exist numerous design methodologies to control nonlinear systems. [6, 7] The analysis and design of nonlinear systems are much more difficult than that of the linear one. Nonlinear differential equations usually cannot obtain the closed-form analytical solution unless differential equations are treated specially, for example, Laplace transform, Fourier transform and Superposition principle which apply to linear systems are not suitable in nonlinear control problems. Therefore, the simplest method to deal with this problem is the linearization of the nonlinear dynamic characteristics. The commonly method is to approximate nonlinear measurement and state transition equations by a Taylor series expansion about an operating point and use standard linear estimation techniques. [8] In this case, the first derivative of the nonlinear function, evaluated at a specific operating point, is used to develop a first order set of linear state equations, such as piecewise linearization, linear parameter-varying modeling method and so on.

The piecewise linear modelling method covered the expected range of the state variables, and this method did not limit the large signal behavior of the modeled states. The only restriction is that the nonlinearities must be able to be approximated as piecewise linear functions. Assuming that the nonlinearities are broken up into several individual linear functions, this may result in individual system, inputs, and outputs and feed forward matrices. The boundaries of the piecewise linear functions may be a function of one state variable or more. The boundary functions are used to select the appropriate system, inputs and gain matrices for the system by using a data selector or a multiplexer. Thus, the piecewise linear model dynamically switches from one set of system and gain matrices to another as the estimated states traverse through their trajectories. And the method used Gauss's least squares regression to determine the coefficients of the linear functions. This method gives the best estimation for each of the regions but suffers from discontinuities at the boundaries of the regions.

One decade ago, linear parameter-varying (LPV) systems [9] were introduced into the context of gain scheduling. It explicitly takes into account the relationship between real-time parameter variations and performance. The synthesis of LPV systems can incorporate the operating conditions into the scheduling parameter of the system to build a controller that is directly parameter dependent, eliminating the explicit mapping of linear controllers. The controller synthesis of LPV systems has drawn much attention in the literatures. In terms of an LPV system, the method of obtaining a controller is fairly straightforward. However, the problem of how to end up in an LPV description of the nonlinear system is far from straightforward. A standard approach to this problem is an approximation of the nonlinear system by mapping Taylor linearization for different operating conditions. It is clear that such LPV models can deviate much from the nonlinear model, and the LPV design may perform badly or even result in an unstable closed-loop system of the original nonlinear system. [10] However, this procedure is motivated under the assumption of slowly varying parameters. Other approaches are to use nonlinear transformations, to obtain an LPV description of the nonlinear systems. [11-13] An LPV system is a linear differential inclusion. This means that a trajectory of the nonlinear system is one possible trajectory of the LPV system, among an infinite number of possibilities. Hence, there is an inherit conservatism in the LPV controller synthesis procedure. Since an LPV description of a nonlinear system is not unique, there is a potential in reducing the conservatism by the choice of LPV description. [14-21]

In this paper, an improved hybrid Kalman filter algorithm is provided, and the benefit of this method is investigated

in a simulation environment. The Kalman filter is a hybrid structure consisted of a nonlinear on-board model (NOBM) and velocity-based LPV (VLPV) models which include Kalman gain matrices. The NOBM is a physics-based model designed to run in real time, while the VLPV model is derived off-line from the NOBM at the nominal health baseline. These two main components are merged together to form the hybrid Kalman filter. The outline of this paper is as follows. First, an improved Kalman filter design procedure is described in Section 2. Section 3 shows the application to two-shaft turbofan engine and simulations. Finally, the conclusion can be obtained in the final section.

2. An improved Kalman filter design procedure

2.1 Linearized continuous Kalman filter

Suppose that the nonlinear system can be described as

$$\begin{cases} \dot{\boldsymbol{x}} = \boldsymbol{f}(\boldsymbol{x},\boldsymbol{u}) + \boldsymbol{w} \\ \boldsymbol{y} = \boldsymbol{g}(\boldsymbol{x},\boldsymbol{u}) + \boldsymbol{v} \end{cases}, \tag{1}$$

where $\boldsymbol{f}(\cdot,\cdot)$ and $\boldsymbol{g}(\cdot,\cdot)$ are differentiable nonlinear functions with Lipschitz continuous first derivatives, and $\boldsymbol{u} \in \Re^m$ denotes the inputs, $\boldsymbol{y} \in \Re^p$ is the outputs and $\boldsymbol{x} \in \Re^n$ represents the states of the system. $\boldsymbol{w}$ is a white process noise signal and $\boldsymbol{v}$ is a white measurement noise one. There is a process noise matrix $\boldsymbol{Q}$ related to the process noise column vector $\boldsymbol{w}$

$$\boldsymbol{Q} = E[\boldsymbol{w}\boldsymbol{w}^T]. \tag{2}$$

And the measurement noise matrix $\boldsymbol{R}$ related to the measurement noise vector $\boldsymbol{v}$

$$\boldsymbol{R} = E[\boldsymbol{v}\boldsymbol{v}^T]. \tag{3}$$

The linearized model with respect to an equilibrium point of Eq.(1) is

$$\begin{cases} \dot{\boldsymbol{x}} = \boldsymbol{A}\boldsymbol{x} + \boldsymbol{B}\boldsymbol{u} + \boldsymbol{w} \\ \boldsymbol{y} = \boldsymbol{C}\boldsymbol{x} + \boldsymbol{v} \end{cases}, \tag{4}$$

where $\boldsymbol{A}$ is the system state matrix, $\boldsymbol{B}$ is the system input matrix and $\boldsymbol{C}$ is the measurement one. The Kalman gain is derived based on the matrix pair $[\boldsymbol{A}\ \ \boldsymbol{C}]$, which must be observable. The resultant continuous Kalman filter is described by the matrix differential equation is

$$\dot{\hat{\boldsymbol{x}}} = \boldsymbol{A}\hat{\boldsymbol{x}} + \boldsymbol{B}\boldsymbol{u} + \boldsymbol{K}(\boldsymbol{y} - \boldsymbol{C}\hat{\boldsymbol{x}}). \tag{5}$$

State propagation of Kalman filter is accomplished by numerically integrating the matrix differential equation involving the system state matrix. The Kalman filter gain, $\boldsymbol{K}$, required by the preceding Kalman-filtering differential equation, is now obtained by first integrating the nonlinear matrix differential Riccati equation for the covariance matrix

$$\dot{\boldsymbol{P}} = -\boldsymbol{P}\boldsymbol{C}^T\boldsymbol{R}^{-1}\boldsymbol{C}\boldsymbol{R} + \boldsymbol{P}\boldsymbol{A}^T + \boldsymbol{A}\boldsymbol{P} + \boldsymbol{Q}, \tag{6}$$

and then solving the matrix equation for the gain in terms of the covariance matrix or

$$\boldsymbol{K} = \boldsymbol{P}\boldsymbol{C}^T\boldsymbol{R}^{-1}. \tag{7}$$

In the continuous Riccati equation, there are two sources of uncertainty involved, which are the covariance matrices $\boldsymbol{Q}$ and $\boldsymbol{R}$. If the correctness of the model needs to be quantified, its uncertainty as part of its behavior (i.e., characterized by the process noise $\boldsymbol{Q}$) should be included. The process noise can directly influence the estimates. The measurement noise $\boldsymbol{R}$ is determined by the actual sensor noise measurement, and the filter will compute the best estimates by the consideration of the sensor noise statistics. The $\boldsymbol{R}$ is an aid to estimating the states. In the filtering equation, the filter gain $\boldsymbol{K}$ operates on the difference between a measurement and the prior estimate of what the measurement should be. Consequently, a larger $\boldsymbol{Q}$ increases $\boldsymbol{P}$; which results in a larger $\boldsymbol{K}$, whereas a larger $\boldsymbol{R}$ tends to decrease $\boldsymbol{K}$. A decreased $\boldsymbol{K}$ does not weight the measurement as much because it is noisy, whereas a larger $\boldsymbol{K}$ (caused by more $\boldsymbol{Q}$) causes more of the measurement to be incorporated in the estimate. It will be seen that this logic leads directly to the concept of how filter bandwidth is determined (i.e., larger $\boldsymbol{Q}$ or smaller $\boldsymbol{R}$ will increase the filter bandwidth, whereas smaller $\boldsymbol{Q}$ or larger $\boldsymbol{R}$ will decrease the filter bandwidth).

2.2 Hybrid Kalman filter structure

To achieve a real-time unmeasured parameters capacity, a hybrid Kalman filter structure is introduced and shown in Fig. 1. At a performance baseline ($\boldsymbol{x}_{ss}$, $\boldsymbol{u}_{ss}$, $\boldsymbol{y}_{ss}$, $\boldsymbol{h}_{ref}$), state variable model can be described as

$$\begin{cases} \Delta\dot{\boldsymbol{x}} = \boldsymbol{A}\Delta\boldsymbol{x} + \boldsymbol{B}\Delta\boldsymbol{u} + \boldsymbol{L}\Delta\boldsymbol{h} + \boldsymbol{v} \\ \Delta\boldsymbol{y}_m = \boldsymbol{C}\Delta\boldsymbol{x} + \boldsymbol{D}\Delta\boldsymbol{u} + \boldsymbol{M}\Delta\boldsymbol{h} + \boldsymbol{w} \end{cases}, \tag{8}$$

where $\Delta\boldsymbol{x}=\boldsymbol{x}-\boldsymbol{x}_{ss}$, $\Delta\boldsymbol{u}=\boldsymbol{u}-\boldsymbol{u}_{ss}$, $\Delta\boldsymbol{y}_m=\boldsymbol{y}_m-\boldsymbol{y}_{ss}$, $\Delta\boldsymbol{h}=\boldsymbol{h}-\boldsymbol{h}_{ref}$, $\boldsymbol{h}$ presents the performance degradation factor, and $\boldsymbol{A}$, $\boldsymbol{B}$, $\boldsymbol{C}$, $\boldsymbol{D}$, $\boldsymbol{L}$, $\boldsymbol{M}$ are system matrices which can be obtained from partial derivative method [22]. In order to estimate $\Delta\boldsymbol{h}$ via $\Delta\boldsymbol{y}_m$, state variable model in Kalman filter should be augmented

$$\begin{cases} \Delta\dot{\boldsymbol{x}}_{aug} = \boldsymbol{A}_{aug}\Delta\boldsymbol{x}_{aug} + \boldsymbol{B}_{aug}\Delta\boldsymbol{u} + \boldsymbol{v} \\ \Delta\boldsymbol{y} = \boldsymbol{C}_{aug}\Delta\boldsymbol{x}_{aug} + \boldsymbol{D}_{aug}\Delta\boldsymbol{u} + \boldsymbol{w} \end{cases}, \tag{9}$$

where $\Delta\boldsymbol{x}_{aug} = \begin{bmatrix} \Delta\boldsymbol{x} \\ \Delta\boldsymbol{h} \end{bmatrix}$, $\boldsymbol{A}_{aug} = \begin{bmatrix} \boldsymbol{A} & \boldsymbol{L} \\ \boldsymbol{0} & \boldsymbol{0} \end{bmatrix}$, $\boldsymbol{B}_{aug} = \begin{bmatrix} \boldsymbol{B} \\ \boldsymbol{0} \end{bmatrix}$,

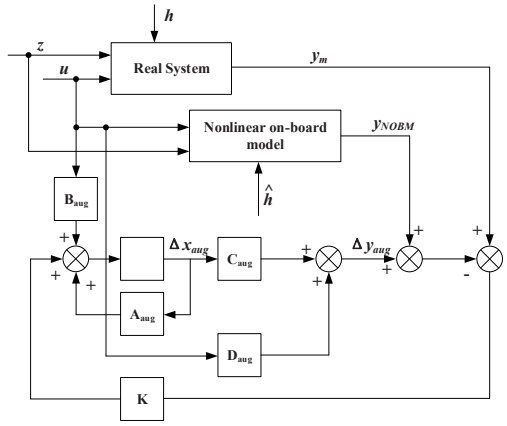

Fig. 1. Framework of the hybrid Kalman filter

$\boldsymbol{C}_{aug} = \begin{bmatrix} \boldsymbol{C} & \boldsymbol{M} \end{bmatrix}$, $\boldsymbol{D}_{aug} = \boldsymbol{D}$. After optimal estimating by Kalman filter, Eq.(10) can be obtained

$$\begin{cases} \Delta\dot{\hat{\boldsymbol{x}}}_{aug} = \boldsymbol{A}_{aug}\Delta\hat{\boldsymbol{x}}_{aug} + \boldsymbol{B}_{aug}\Delta\boldsymbol{u} + \boldsymbol{K}(\Delta\boldsymbol{y}_m - \Delta\hat{\boldsymbol{y}}_m) \\ \Delta\hat{\boldsymbol{y}}_m = \boldsymbol{C}_{aug}\Delta\hat{\boldsymbol{x}}_{aug} + \boldsymbol{D}_{aug}\Delta\boldsymbol{u} \end{cases}, \tag{10}$$

where $\boldsymbol{K}$ is Kalman gain matrix which is obtained by Eq. (7). Now the outputs of NOBM (shown in Fig. 1 Nonlinear on-board model), are used for the baseline of Kalman filter, which means the baseline in Eq. (10) is ($\boldsymbol{x}_{NOBM}$, $\boldsymbol{u}$, $\boldsymbol{y}_{NOBM}$, $\boldsymbol{h}_{NOBM}$) instead of ($\boldsymbol{x}_{ss}$, $\boldsymbol{u}_{ss}$, $\boldsymbol{y}_{ss}$, $\boldsymbol{h}_{ref}$). Where in subscript 'NOBM' means nonlinear on-board model shown in Fig. 1.

$$\begin{cases} \Delta\dot{\hat{\boldsymbol{x}}}_{aug} = \boldsymbol{A}_{aug}\Delta\hat{\boldsymbol{x}}_{aug} + \boldsymbol{B}_{aug}\Delta\boldsymbol{u} + \boldsymbol{K}(\boldsymbol{y}_m - \hat{\boldsymbol{y}}_m) \\ \hat{\boldsymbol{y}}_m = \boldsymbol{C}_{aug}\Delta\hat{\boldsymbol{x}}_{aug} + \boldsymbol{D}_{aug}\Delta\boldsymbol{u} + \boldsymbol{y}_{NOBM} \end{cases}. \tag{11}$$

2.3 Kalman filter based on a velocity-based LPV framework

The requirements of higher stability and maneuvering performance for nonlinear systems, more significant dynamic characteristics due to facts such as various coupling effects, strong nonlinearities, extreme ranges of operating conditions and rapid changes of mass distribution. Therefore, seeking better control-oriented model and designing more appropriate controller of hypersonic vehicles are one of the major tasks in developing hypersonic vehicle technologies.

In this section, the velocity-based LPV modeling approach is briefly reviewed. Considering a general nonlinear system

$$\begin{cases} \dot{\boldsymbol{x}}(t) = \boldsymbol{f}(\boldsymbol{x}(t), \boldsymbol{u}(t)) \\ \boldsymbol{y}(t) = \boldsymbol{g}(\boldsymbol{x}(t), \boldsymbol{u}(t)) \end{cases}, \tag{12}$$

where $\boldsymbol{f}(\cdot,\cdot)$ and $\boldsymbol{g}(\cdot,\cdot)$ are differentiable nonlinear functions with Lipschitz continuous first derivatives, and $\boldsymbol{u}(t) \in \Re^m$ denotes the input to the plant, $\boldsymbol{y}(t) \in \Re^p$ the output and $\boldsymbol{x}(t) \in \Re^n$ the state. The goal is to find a set of differential equations having the LPV form

$$\begin{cases} \dot{\boldsymbol{x}}(t) = \boldsymbol{A}(\boldsymbol{\rho}(t))\boldsymbol{x}(t) + \boldsymbol{B}(\boldsymbol{\rho}(t))\boldsymbol{u}(t) \\ \boldsymbol{y}(t) = \boldsymbol{C}(\boldsymbol{\rho}(t))\boldsymbol{x}(t) + \boldsymbol{D}(\boldsymbol{\rho}(t))\boldsymbol{u}(t) \end{cases}. \tag{13}$$

where $\boldsymbol{\rho}(t)$ is the parameter vector or scheduling variable of the system which is not known in advance but can be measured or estimated in real-time, such that the solution of Eq.(12) is as close to the solution of Eq.(13) as possible in a predefined region of $\boldsymbol{\rho}(t) \in \Im \subseteq \Re^{\Im}$. Given an LPV system a predefined in Eq.(13), if a scheduling variable $\boldsymbol{\rho}(t)$ is also a state of the system, then this particular class of systems is called quasi-LPV systems, and the framework is shown in Fig. 2.

What has become a standard way of obtaining an LPV model of the form Eq.(13) is to linearize the nonlinear system Eq.(12) in different equilibrium operating points and map the linearization together to achieve an LPV system. There is, however, no direct connection between the nonlinear system and the obtained LPV system. Other methods like analytical transformation are inadequate whenever the nonlinear system is of high order and/or contain look-up tables. The velocity-based linearization developed by Leith and Leithead [23] offers both a theoretical relation of the LPV system and the nonlinear one, and is applicable to more complicated system using numerical methods. The basic idea of velocity-based linearization is to make a differentiation of Eq.(12) in time, an alternative representation of the nonlinear system is

$$\begin{cases} \ddot{\boldsymbol{x}}(t) = \boldsymbol{A}(\boldsymbol{\rho}(t))\dot{\boldsymbol{x}}(t) + \boldsymbol{B}(\boldsymbol{\rho}(t))\dot{\boldsymbol{u}}(t) \\ \dot{\boldsymbol{y}}(t) = \boldsymbol{C}(\boldsymbol{\rho}(t))\dot{\boldsymbol{x}}(t) + \boldsymbol{D}(\boldsymbol{\rho}(t))\dot{\boldsymbol{u}}(t) \end{cases}, \tag{14}$$

where

$$\boldsymbol{A}(\boldsymbol{\rho}(t)) = \frac{\partial \boldsymbol{f}}{\partial \boldsymbol{x}}(\boldsymbol{x}(t), \boldsymbol{u}(t)), \quad \boldsymbol{B}(\boldsymbol{\rho}(t)) = \frac{\partial \boldsymbol{f}}{\partial \boldsymbol{u}}(\boldsymbol{x}(t), \boldsymbol{u}(t)),$$

$$\boldsymbol{C}(\boldsymbol{\rho}(t)) = \frac{\partial \boldsymbol{g}}{\partial \boldsymbol{x}}(\boldsymbol{x}(t), \boldsymbol{u}(t)), \quad \boldsymbol{D}(\boldsymbol{\rho}(t)) = \frac{\partial \boldsymbol{g}}{\partial \boldsymbol{u}}(\boldsymbol{x}(t), \boldsymbol{u}(t)).$$

It is noted that the velocity-based linearization system Eq.(14) is not an approximation for the original system Eq.(12), however, holds exactly. That is, the linearization system Eq.(14) is equivalent to the original nonlinear system Eq.(12). Moreover, the velocity-based linearization is hold at

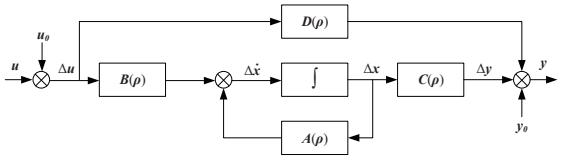

Fig. 2. Framework of LPV modeling

every operating point and not just the equilibrium operating points, and the framework is shown in Fig. 3.

Kalman gains are derived based on the linear representations of the nonlinear system. When implemented, however, linear models and associated Kalman gains are integrated with the nonlinear system model.

$$\begin{cases} \dot{\boldsymbol{x}}_1 = \boldsymbol{A}(\boldsymbol{\rho})\boldsymbol{x}_1 + \boldsymbol{B}(\boldsymbol{\rho})\dot{\boldsymbol{u}} + \boldsymbol{w} \\ \dot{\boldsymbol{y}} = \boldsymbol{C}(\boldsymbol{\rho})\boldsymbol{x}_1 + \boldsymbol{D}(\boldsymbol{\rho})\dot{\boldsymbol{u}} + \boldsymbol{v} \end{cases}, \tag{15}$$

where $\boldsymbol{x}_1 = \dot{\boldsymbol{x}}$ is a column vector with the states of the system, $\boldsymbol{A}(\boldsymbol{\rho})$ the system dynamics matrix scheduled by $\boldsymbol{\rho}$.

$$\begin{cases} \dot{\hat{\boldsymbol{x}}}_1 = \boldsymbol{A}(\boldsymbol{\rho})\hat{\boldsymbol{x}}_1 + \boldsymbol{B}(\boldsymbol{\rho})\dot{\boldsymbol{u}} + \boldsymbol{K}(\boldsymbol{\rho})(\dot{\boldsymbol{y}} - \dot{\hat{\boldsymbol{y}}}) \\ \dot{\hat{\boldsymbol{y}}} = \boldsymbol{C}(\boldsymbol{\rho})\hat{\boldsymbol{x}}_1 + \boldsymbol{D}(\boldsymbol{\rho})\dot{\boldsymbol{u}} \end{cases}, \tag{16}$$

where $\boldsymbol{K}(\boldsymbol{\rho})$ is Kalman filter gains

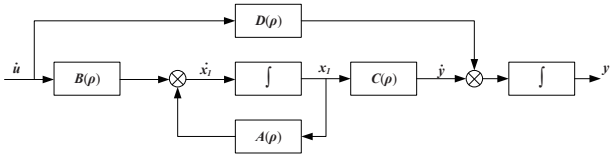

Fig. 3. Framework of velocity-based LPV modeling

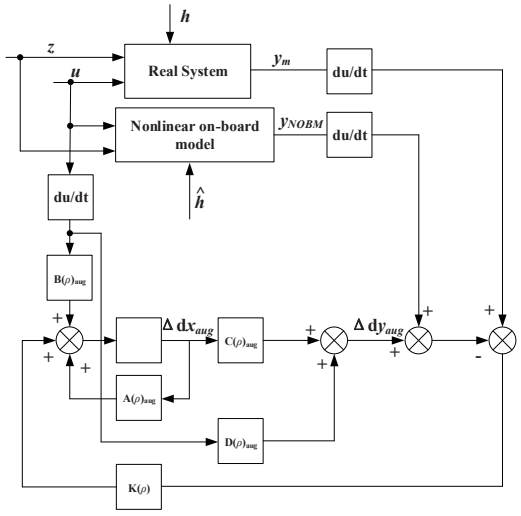

Fig. 4. Framework of the improved hybrid Kalman filter

$$\boldsymbol{K}(\boldsymbol{\rho}) = \boldsymbol{P}(\boldsymbol{\rho})\boldsymbol{C}(\boldsymbol{\rho})^T \boldsymbol{R}^{-1}, \tag{17}$$

and $\boldsymbol{P}(\boldsymbol{\rho})$ are solutions of the Riccati equation

$$\boldsymbol{A}(\boldsymbol{\rho})\boldsymbol{P}(\boldsymbol{\rho}) + \boldsymbol{P}(\boldsymbol{\rho})\boldsymbol{A}^T(\boldsymbol{\rho}) - \boldsymbol{P}(\boldsymbol{\rho})\boldsymbol{C}(\boldsymbol{\rho})^T \boldsymbol{R}^{-1}\boldsymbol{C}(\boldsymbol{\rho})\boldsymbol{P}(\boldsymbol{\rho}) + \boldsymbol{Q} = \boldsymbol{0}. \tag{18}$$

The process of model design is shown as follow:

1) Providing the aero-thermodynamic component-level model as NOBM.
2) Defining a plurality of steady-state points in the whole flight envelop.
3) Building the VLPV model and Kalman gain matrix at each point and combining them to Kalman filters.
4) Defining the scheduled parameters and uniting all points to VLPV Kalman filter, 5) Combining NOBM and VLPV Kalman filter into the architecture.

The hybrid Kalman filter based on a velocity-based LPV framework is shown in Fig. 4.

3. Simulations and applications

The aircraft engine model used in this paper is a nonlinear component-level model of an advanced high-bypass two-spool turbofan engine, a typical power plant for large commercial aircraft. The schematic configuration of the turbofan engine is shown in Fig. 5. The high pressure compressor (HPC) and high pressure turbine (HPT) are on one shaft (driven by the high speed rotor), while the fan, booster and low pressure tur-bine (LPT) are on the other shaft (driven by the low speed rotor). Bleed effects (for air bleed from the booster and the compressor) are not currently considered in the model [24].

The nonlinear functions of aircraft gas turbine engine is represented in the following form

$$\begin{cases} \dot{\boldsymbol{x}} = \boldsymbol{f}(\boldsymbol{x}, \boldsymbol{h}, \boldsymbol{\rho}, \boldsymbol{u}, \boldsymbol{w}) \\ \boldsymbol{y} = \boldsymbol{g}(\boldsymbol{x}, \boldsymbol{h}, \boldsymbol{\rho}, \boldsymbol{u}, \boldsymbol{w}) + \boldsymbol{v} \end{cases}, \tag{19}$$

where $\boldsymbol{x}$, $\boldsymbol{h}$, $\boldsymbol{\rho}$, $\boldsymbol{u}$, and $\boldsymbol{w}$ represent the vectors of state variables, health parameters, scheduling parameters, control command inputs, and environmental parameters, respectively. During given inputs, the nonlinear functions

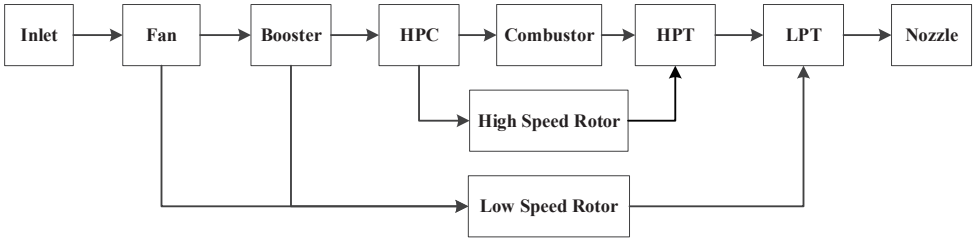

Fig. 5. Schematic configuration of two-spool turbofan engine

$\boldsymbol{f}$ and $\boldsymbol{g}$ will generate the vectors of state derivatives $\dot{\boldsymbol{x}}$ and measurement output $\boldsymbol{y}$. The sensor outputs are corrupted by the white noise vector $\boldsymbol{v}$.

By linearizing the engine model at a given operation point, the corresponding linear state-space equations are obtained

$$\begin{cases} \dot{\boldsymbol{x}}_1 = \boldsymbol{A}(\boldsymbol{\rho})\boldsymbol{x}_1 + \boldsymbol{B}(\boldsymbol{\rho})\dot{\boldsymbol{u}} + \boldsymbol{L}(\boldsymbol{\rho})\boldsymbol{h} + \boldsymbol{w} \\ \boldsymbol{y} = \boldsymbol{C}(\boldsymbol{\rho})\boldsymbol{x}_1 + \boldsymbol{D}(\boldsymbol{\rho})\dot{\boldsymbol{u}} + \boldsymbol{M}(\boldsymbol{\rho})\boldsymbol{h} + \boldsymbol{v} \end{cases}, \tag{20}$$

where $\boldsymbol{x}=[n_H\ n_L]^T$, $\boldsymbol{x}_1=\dot{\boldsymbol{x}}$, $\boldsymbol{h}=[DC_{EF}\ DC_{EB}\ DC_{EC}\ DC_{WF}\ DC_{WB}\ DC_{WC}]^T$, $\boldsymbol{y}=\begin{bmatrix} n_H & n_L & EGT \end{bmatrix}^T$, $\boldsymbol{u}=w_{mf}$. $\boldsymbol{A}$, $\boldsymbol{B}$, $\boldsymbol{C}$, $\boldsymbol{D}$, $\boldsymbol{L}$ and $\boldsymbol{M}$ are the state-space matrices scheduled by $\boldsymbol{\rho}$ with appropriate dimensions. In this paper, the improved hybrid Kalman filter is established based on the state-space equations at different operation points, and n_H is chosen as the scheduling parameter $\boldsymbol{\rho}$ of the VLPV structure. There are functions between the elements of state-space matrices and the scheduling parameter, and the elements of state-space matrices will be tuned in parallel with the variation of the $\boldsymbol{\rho}$, Fig. 6 shows an example.

Considering that the length of the paper is limited, an example of Kalman filter corre-sponding to one operation point is shown in this paper. The operation point of the engine is x=[6920 3682]^T, and the corresponding matrices are:

$$A = \begin{bmatrix} \text{-5.9555}e\text{-1} & \text{-3.2675e-1} & \text{7.2190e1} & \text{-6.6833e3} & \text{-8.4614e3} & \text{-1.6744e1} \\ \text{3.4872e-1} & \text{-1.0403} & \text{-2.0246e3} & \text{3.5306e2} & \text{3.5548e2} & \text{-2.1750e3} \\ 0 & 0 & 0 & 0 & 0 & 0 \\ 0 & 0 & 0 & 0 & 0 & 0 \\ 0 & 0 & 0 & 0 & 0 & 0 \\ 0 & 0 & 0 & 0 & 0 & 0 \end{bmatrix},$$

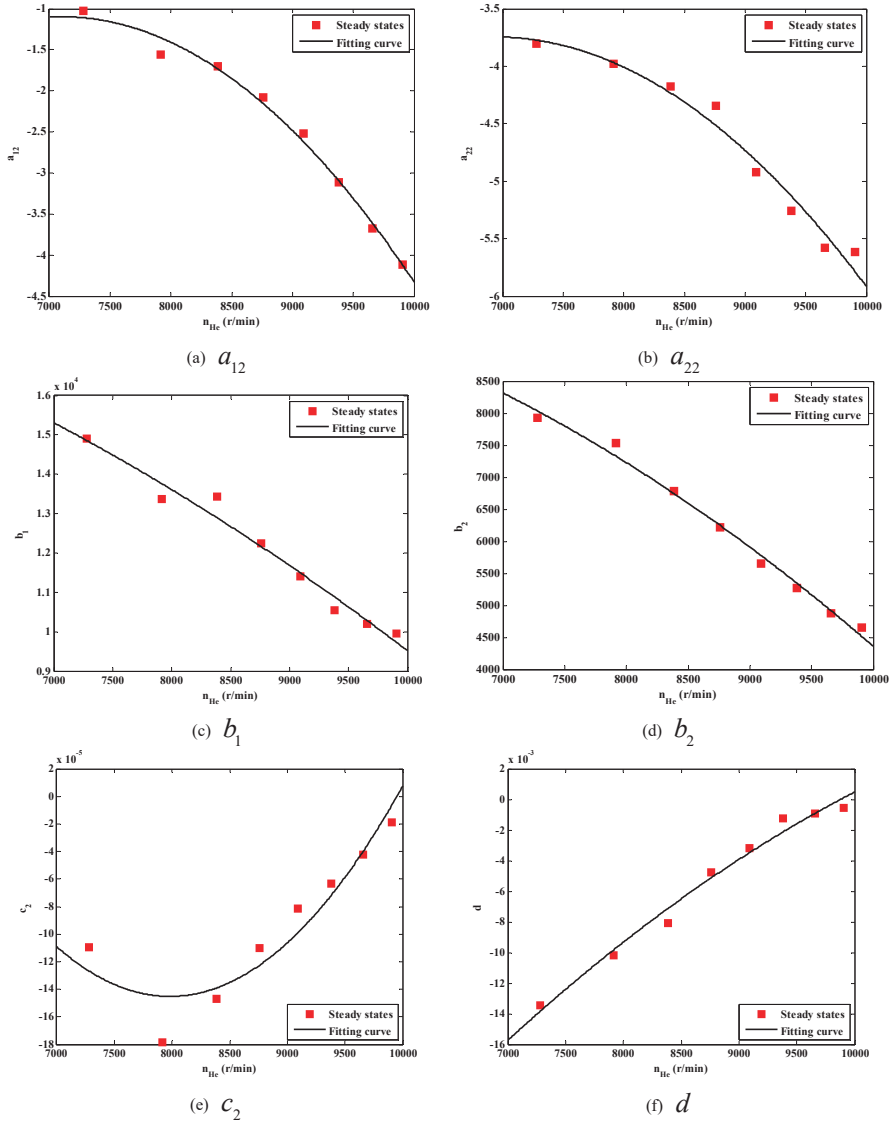

(a) a_{12} (b) a_{22} (c) b_1 (d) b_2 (e) c_2 (f) d

Fig. 6. Fitting results of the EME model partial items by $\rho = n_H$

$$C=\begin{bmatrix} 1 & 0 & 0 & 0 & 0 & 0 \\ 0 & 1 & 0 & 0 & 0 & 0 \\ -1.9975e\text{-}4 & 7.9158e\text{-}3 & 1.7281e1 & 1.0851e\text{-}1 & 1.1191e\text{-}1 & -9.9153e\text{-}3 \\ -2.7605e\text{-}1 & 9.6362 & 5.1711e2 & 1.5631e2 & 1.6452e2 & -5.7998 \\ 3.3112e\text{-}2 & 2.2213e\text{-}2 & 2.4988e1 & 2.9336e2 & 2.8507e\text{-}1 & 4.9636e\text{-}4 \\ 1.2545e2 & 1.4453e2 & -3.8159e4 & 5.2069e4 & -8.1884e4 & -5.4656e2 \end{bmatrix}$$

and

$$P=\begin{bmatrix} 2.7687e4 & -3.7238e3 & 1.6066e1 & -2.2022e1 & 1.4089e1 & -7.9049e\text{-}1 \\ -3.7238e3 & 3.6662e3 & -1.0028e1 & -3.2553 & 3.3513 & 4.6983 \\ 1.6606e1 & -1.0028e\text{-}4 & 2.6593e\text{-}5 & -1.7107e\text{-}4 & 1.7806e\text{-}4 & -4.9549e\text{-}5 \\ -22.0222 & -3.25529 & 4.6174e\text{-}2 & 4.4899e\text{-}2 & -3.1945e\text{-}2 & -4.3312e\text{-}2 \\ 1.4089e1 & 3.3513 & -3.6636e\text{-}2 & -3.1945e\text{-}2 & 2.4349e\text{-}2 & 3.2363e\text{-}2 \\ -7.0949 & 4.6983 & -1.3572e\text{-}1 & -4.3313e\text{-}2 & 3.2363e\text{-}2 & 1.2449e\text{-}1 \end{bmatrix},$$

$$K=\begin{bmatrix} 2.7688e\text{-}1 & -3.7238e\text{-}2 & 2.4189e\text{-}3 & -3.6301e\text{-}1 & -5.2211e\text{-}2 & 2.5885e\text{-}1 \\ -3.7238e\text{-}2 & -3.6662e\text{-}2 & 1,4355e\text{-}3 & 3.1186e01 & -1.2464e\text{-}2 & -1.1413e\text{-}2 \\ 1.6606e\text{-}4 & -1.0028e\text{-}4 & 2.6593e\text{-}5 & -1.7107e\text{-}4 & 1.7806e\text{-}4 & -4.9549e\text{-}5 \\ -2.2022e\text{-}4 & -3.2553e\text{-}5 & 7.7828e\text{-}6 & 6.0134e\text{-}6 & 1.3515e\text{-}4 & -1.7911e\text{-}4 \\ 1.4089e\text{-}4 & 3.3513e\text{-}5 & -6.1045e\text{-}6 & 8.2847e\text{-}5 & -9.7390e\text{-}5 & -2.5028e\text{-}4 \\ -7.0949e\text{-}5 & 4.6983e\text{-}5 & -2.3091e\text{-}5 & -2.5119e\text{-}4 & -1.6219e\text{-}4 & -5.3121e\text{-}5 \end{bmatrix}.$$

Firstly, the stability of the improved hybrid Kalman filter is evaluated. According to Eqs. (17) and (18), the performance of Kalman filter is conducted by the metrics $\boldsymbol{Q}$ and $\boldsymbol{R}$. According to the theory put forward by Zarchan Paul[25], the use of comparative theoretical error and the actual error of the Kalman filter can evaluate the job performance of the Kalman filter. That is, for normal operating state Kalman filter, if the actual system state vectors estimation error in the range of theoretical error (±5%) in at least 68% of the total time, the setting of parameters of $\boldsymbol{Q}$ and $\boldsymbol{R}$ can be identified as available.

According to the reference above, the set of $\boldsymbol{Q}$ and $\boldsymbol{R}$ can be evaluated at different values. In these evaluations, with regard to measured noise, the actual sensor standard deviations are probably at 0.1% to 1% in percent of steady-state values at ground maximum condition. For simplification, the standard deviation is assumed at 0.2% in this section.

In order to evaluate the performance of the improved hybrid Kalman filter by setting $\boldsymbol{Q}$ and $\boldsymbol{R}$, the fan efficiency, the improved hybrid Kalman filter can recognize rapidly its change when it drops 1% at t=1s shown in Fig. 7, and the values ranges of $\boldsymbol{Q}$ and $\boldsymbol{R}$ are $\boldsymbol{Q}\in[10,100]$ and $\boldsymbol{R}\in[1,10]$.

The estimation accuracy of the improved hybrid kalman filter is demonstrated in Fig.7. At t=1s the fan efficiency decreases by 1%. The improved hybrid Kalman filter can recognize the variation of the fan efficiency based on the mismatch between the NOBM and the actual engine. The performance degradation factor estimation is successfully completely within 4s.

4. Conclusions

This paper proposes an improved hybrid Kalman filter and describes the model architecture, work mode and the key techniques of model design in details. By applying it to a turbofan engine, a series of simulations are made in synthetic mode. The results show that this model can effectively estimate the real engine performance in the whole flight envelope, different engine states and severe performance deterioration condition. The improved hybrid Kalman filter will be used for in-flight aircraft engine performance estimation, fault detection and isolation, and the further researches will be accomplished based on the Kalman filter of this paper.

Acknowledgement

The author would thank the anonymous reviewers for their critical and constructive review of the manuscript. This study was supported by the National Natural Science Foundation of China.

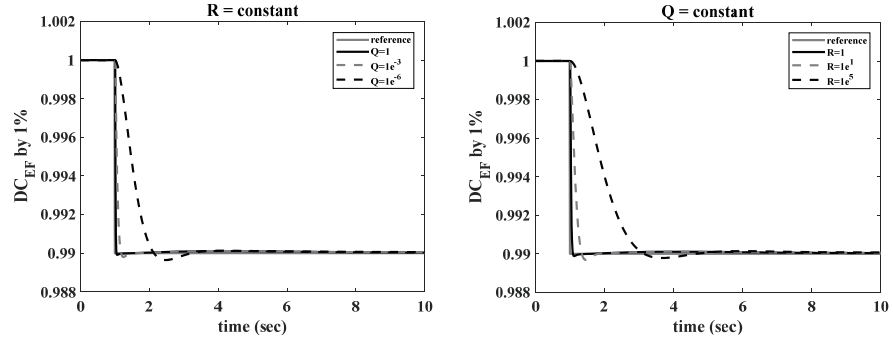

(a) Parameter setting comparison of $\boldsymbol{Q}$ when $\boldsymbol{R}$ is constant (b) Parameter setting comparison of $\boldsymbol{R}$ when $\boldsymbol{Q}$ is constant

Fig. 7. Parameters comparison

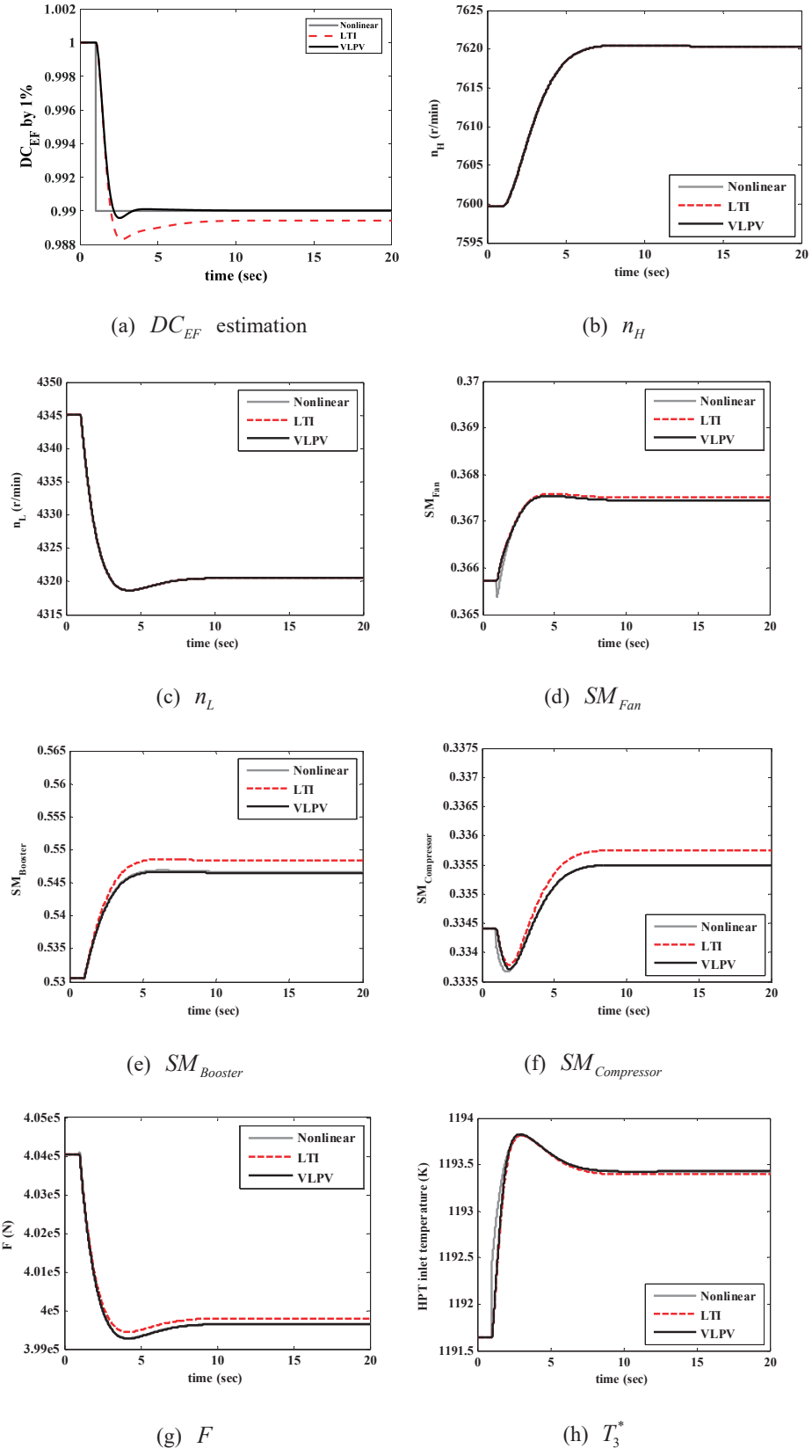

(a) DC_{EF} estimation

(b) n_H

(c) n_L

(d) SM_{Fan}

(e) $SM_{Booster}$

(f) $SM_{Compressor}$

(g) F

(h) T_3^*

Fig. 8. Comparisons of different Kalman filters' estimations with nonlinear model

Notations

symbol	description
$\boldsymbol{x}$	system state variable
$\boldsymbol{y}$	system output variable
$\boldsymbol{u}$	system input variable
$\boldsymbol{w}$	white process noise signal
$\boldsymbol{v}$	white measurement noise signal
$\boldsymbol{Q}$	covariance matrix of $\boldsymbol{w}$
$\boldsymbol{R}$	covariance matrix of $\boldsymbol{v}$
$\boldsymbol{h}$	performance degradation factor
DC	degradation coefficient
n	spool speed (r/min)
EGT	engine exhausted temper-ature (K)
w	mass flow (liter/h)
$\boldsymbol{\rho}$	scheduled parameter
SM	surge margin
F	engine thrust
T_3^*	HPT inlet temperature

subscript	description
aug	augmented system
mf	fuel
m	measured parameter
EF	Fan efficiency
ss	steady state
EB	Booster efficiency
ref	reference value
EC	Compressor efficiency
NOBM	Nonlinear on-board Model
WF	Fan flow capacity
0	initial value
WB	Booster flow capacity
H	high pressure
WC	Compressor flow capacity
L	low pressure

References

[1] Adibhatla, Shrider, et al. “Model-based intelligent digital engine control (MoBIDEC).” Joint Propulsion Conference and Exhibit, 2013.

[2] Simon, Dan, and D. L. Simon. “Aircraft Turbofan Engine Health Estimation Using Constrained Kalman Filtering.” Journal of Engineering for Gas Turbines & Power 127.2, 2003, pp. 1930-4.

[3] Luppold R, Roman J, Gallops G, et al. “Estimating in-flight engine performance variations using Kalman filter concepts”, 25th Joint Propulsion Conference, Joint Propulsion Conferences, 1989.

[4] Volponi, A., D. L. Simon. “Enhanced Self-Tuning On-Board Real-Time Model (eSTORM) for Aircraft Engine Performance Health Tracking.” NASA Technical Report, 2008.

[5] Simon, T.K.D., “Hybrid Kalman Filter: A New Approach for Aircraft Engine In-Flight Diagnostics.” NASA Technical Report, 2006.

[6] Tanizaki, H., “Nonlinear filters: estimation and applications.” Berlin: Springer, Vol. 400. 1996.

[7] Gan, Q. and C.J. Harris, “Fuzzy local linearization and local basis function expansion in nonlinear system modeling.” Systems, Man, and Cybernetics, Part B: Cybernetics, IEEE Transactions on, Vol. 29, Issue 4, 1999, pp. 559-565.

[8] Kailath, T., “Linear systems.” New Jersey: Prentice-Hall Englewood Cliffs, 1980.

[9] Shamma, J.S. and M. Athans, “Gain scheduling: Potential hazards and possible remedies.” Control Systems, Vol. 12 Issue 3, 1992, pp. 101-107.

[10] Leith, D.J. and W.E. Leithead, “On formulating nonlinear dynamics in LPV form, in Proceedings of the 39th IEEE Conference on Decision and Control.” IEEE: Sydney. 2000, pp. 3526-3527.

[11] Sommer, S. and U. Korn. “Modeling a class of nonlinear plants as LPV-systems via nonlinear state-transformation.” in 3rd IMACS symposium on Mathematical Modeling. 2000.

[12] Packard, A. and M. Kantner. “Gain scheduling the LPV way.” Decision and Control, 1996. Proceedings of the, IEEE IEEE Xplore, vol.4, 1997, pp. 3938-3941.

[13] Bruzelius, F. and C. Breitholtz. “Gain scheduling via affine linear parameter-varying systems and H_∞ synthesis.” Decision and Control, 2001. Proceedings of the, IEEE Conference on IEEE, vol. 3, 2001, pp. 2386-2391.

[14] Shamma, J.S. and M. Athans, “Analysis of gain scheduled control for nonlinear plants.” IEEE Transactions on Automatic Control, Vol. 35, Issue 8, 1990, pp. 898-907.

[15] Rugh, W.J., “Analytical framework for gain scheduling.” Control Systems, 1991. Vol.11, Issue 1, 1991, pp. 79-84.

[16] Apkarian, P. and P. Gahinet, “A convex characterization of gain-scheduled H∞ controllers.” IEEE Transactions on Automatic Control, Vol 40, Issue 5, 1995, pp. 853-864.

[17] Whatley, M.J. and D.C. Pott, “Adaptive gain improves reactor control.” Hydrocarbon processing, Vol. 63, Issue 5, 1984. pp. 75-78.

[18] Leith, D.J. and W.E. Leithead, “Survey of gain-scheduling analysis and design." International Journal of Control, Vol. 73, Issue 11, 2000, pp. 1001-1025.

[19] Shamma, J.S., “Analysis and design of gain scheduled control systems.” Massachusetts Institute of Technology,

1988.

[20] Henrion, D., J. Bernussou, and D. Boyer, "Polynomial LPV synthesis applied to turbofan engines." Control Engineering Practice, 2008, pp. 1-7.

[21] Wolodkin, G., G. Balas, and W. Garrard, "Application of Parameter-Dependent Robust Control Synthesis to Turbofan Engines." Journal of Guidance, Control, and Dynamics, Vol. 22, Issue 6, 1998, pp. 833-838.

[22] Liu, X. and L. Zhao, "Approximate Nonlinear Modeling of Aircraft Engine Surge Margin Based on Equilibrium Manifold Expansion." Chinese Journal of Aeronautics, Vol. 25, Issue 5, 2012, pp. 663-674.

[23] Leith, D. and W. Leithead, "Gain-scheduled and nonlinear systems: dynamic analysis by velocity-based linearization families." International Journal of Control, Vol. 70, Issue 2,1998, pp. 289-317.

[24] Liu, X., et al., "Design for Aircraft Engine Multi-objective Controllers with Switching Characteristics." Chinese Journal of Aeronautics, Vol. 27, Issue 5, 2014, pp. 1097-1110.

[25] Musoff, H. and P. Zarchan, "Fundamentals of Kalman Filtering: A Practical Approach, Second Edition." Progress in Astronautics & Aeronautics, Vol. 190, Issue 8, 2005, pp. 83.